Received: 28 November 2022 | Revised: 19 April 2023 | Accepted: 20 April 2023

DOI: 10.1002/kin.21651

INTERNATIONAL JOURNAL OF CHEMICAL KINETICS WILEY

RESEARCH ARTICLE

Kinetics of the cross-reaction of CH_3O_2 + HO_2 radicals measured in the Highly Instrumented Reactor for Atmospheric Chemistry

Freja F. Østerstrøm[1] | **Lavinia Onel**[1] | **Alexander Brennan**[1] | **Joseph M. Parr**[1] | **Lisa K. Whalley**[1,2] | **Paul W. Seakins**[1] | **Dwayne E. Heard**[1]

[1]School of Chemistry, University of Leeds, Leeds, UK

[2]National Centre for Atmospheric Science, University of Leeds, UK

Correspondence
Freja F. Østerstrøm and Dwayne E. Heard, School of Chemistry, University of Leeds, LS2 9JT Leeds, UK.
Email: freja@chem.ku.dk and d.e.heard@leeds.ac.uk

Present addresses
Freja F. Østerstrøm, School of Engineering and Applied Sciences, Harvard University, Cambridge, MA 02138, USA
Department of Chemistry, University of Copenhagen, 2100 Copenhagen Ø, Denmark
Joseph M. Parr, Department of Chemistry, Imperial College London, W12 0BZ London, UK

Funding information
Natural Environment Research Council (NERC), Grant/Award Number: NE/M011208/1; National Centre for Atmospheric Science; NERC SPHERES doctoral training programme, Grant/Award Number: NE/L002574/1; Carlsberg Foundation Internationalisation Fellowship, Grant/Award Numbers: CF16-0493, CF17-0608

Abstract

The sensitive Fluorescence Assay by Gas Expansion (FAGE) method has been used to detect methyl peroxy (CH_3O_2) and hydroperoxyl (HO_2) radicals after their conversion by titration with excess NO to methoxy (CH_3O) and hydroxyl (OH) radicals, respectively, to study the kinetics of the reaction of CH_3O_2 + HO_2 radicals. The rate coefficient of the reaction was measured in the Highly Instrumented Reactor for Atmospheric Chemistry (HIRAC) at 1000 mbar of synthetic air at T = 268–344 K, selectively detecting both radicals. Using a numerical model to fit both CH_3O_2 and HO_2 radical temporal decays globally at each temperature investigated, rate coefficients for the reaction have been obtained. The room temperature rate coefficient was found to be $k_{CH3O2+HO2}(295\ K) = (4.6 \pm 0.7) \times 10^{-12}$ molecule^{-1} cm^3 s^{-1} (2σ errors) and the temperature dependence of the rate coefficient can be characterized in Arrhenius form by $k_{CH3O2+HO2}(268\ K < T < 344\ K) = (5.1 \pm 2.1) \times 10^{-13} \times \exp((637 \pm 121)/T)$ cm^3 molecule^{-1} s^{-1}. The rate coefficients obtained here are 14%–16% lower than the literature recommended values with an uncertainty which is reduced significantly compared to previous reports.

KEYWORDS
gas phase reactions, global fitting, kinetics, radical-radical reactions, temperature dependence

1 | INTRODUCTION

Methyl peroxy (CH_3O_2) and hydroperoxyl (HO_2) radicals are important intermediate species in atmospheric oxidation and in the combustion of volatile organic compounds (VOCs).[1–3] HO_2 is central in the HO_x ($HO_x = OH + HO_2$) chemical cycle, part of the daytime oxidative chemistry of the atmosphere, with an average daytime concentration of about 1×10^8 molecule cm^{-3}.[4–6] CH_3O_2 is the most abundant organic peroxy (RO_2) radical in the atmosphere, with estimated atmospheric concentrations from box modeling of about $(0.5–6) \times 10^8$ molecule cm^{-3}, depending on the regional environment.[4–6] HO_2 radicals are formed in the OH- or O_3-initiated oxidation of hydrocarbons in the atmosphere and CH_3O_2 radicals are mainly formed through the reaction of methane (CH_4) with hydroxyl radicals (OH):

$$CH_4 + OH \rightarrow CH_3 + H_2O \quad (1)$$

$$CH_3 + O_2 \xrightarrow{M} CH_3O_2 \quad (2)$$

In more polluted tropospheric environments, the removal of CH_3O_2 is mostly dominated by the reaction with NO, governed by the availability of NO_x ($NO_x = NO + NO_2$) in the atmosphere and hence influenced predominantly by anthropogenic emissions, converting NO to NO_2 (an important step in tropospheric ozone production):

$$CH_3O_2 + NO \rightarrow CH_3O + NO_2 \quad (3)$$

The methoxy radical (CH_3O) formed reacts with O_2 to produce HO_2 and formaldehyde (CH_2O); HO_2 then reacts with an additional NO to form a second NO_2 molecule:

$$CH_3O + O_2 \rightarrow CH_2O + HO_2 \quad (4)$$

$$HO_2 + NO \rightarrow OH + NO_2 \quad (5)$$

During the daytime, NO_2 photolysis is the main source of tropospheric ozone (O_3) which is harmful to human health and contributes to global warming. The World Health Organization (WHO) air quality guidelines recommends that exposure to O_3 pollution should not exceed peak season 8-h mean exposure of 60 $\mu g\ m^{-3}$ and 8-h daily maximum exposure of 100 $\mu g\ m^{-3}$.[7] As can be seen in reactions (3)–(5), CH_3O_2 radicals influence the HO_x and NO_x atmospheric propagation reactions. Under low NO_x conditions, typical of remote environments, but sometimes also encountered in urban environments (<0.05 ppbv NO was observed in the afternoon in the summer of 2017 in Beijing[8]), the loss of CH_3O_2 is dominated by its self-reaction as well as reactions with HO_2 and other RO_2 radicals. The self-reaction of CH_3O_2 radicals proceeds via two channels[9,10]:

$$CH_3O_2 + CH_3O_2 \rightarrow CH_3OH + CH_2O + O_2 \quad (6a)$$

$$CH_3O_2 + CH_3O_2 \rightarrow CH_3O + CH_3O + O_2 \quad (6b)$$

CH_2O formed in channel (6a) is toxic via inhalation and its photolysis provides a source of HO_2, and channel (6b) leads to the formation of HO_2 radicals, as described above in reaction (4). The rate coefficient, k_6, and the branching ratio of the channel forming CH_3O radicals, $\alpha_{6b} = k_{6b}/k_6$, has recently been remeasured by Onel et al.[11] They found $k_6 = (2.0 \pm 0.4) \times 10^{-13}$ cm^3 $molecule^{-1}$ s^{-1} and $\alpha_{6b} = 0.34 \pm 0.02$ at 295 K as well as elucidating the temperature dependence of the rate coefficient and branching ratio. The overall rate coefficient for reaction (6) was found to be ~40% lower than the recommended values by the International Union of Pure and Applied Chemistry (IUPAC)[12] and the Jet Propulsion Laboratory (JPL).[13] Onel et al.[11] suggested that the overestimation by the previous studies[14–21] was caused by secondary chemistry in some experiments and a combination of overestimation of optical properties (absorption coefficients) with unaccounted CH_3O_2 heterogenous losses in other experiments. Onel et al. used a concise kinetic model in the analysis of the experimental CH_3O_2 decays as well as a complex chemical mechanism in a numerical model in the investigation of previous publications on reaction (6).

HO_2 radicals can be removed by their self-reaction, which proceeds via bimolecular or termolecular channels:

$$HO_2 + HO_2 \rightarrow H_2O_2 + O_2 \quad (7a)$$

$$HO_2 + HO_2 \xrightarrow{M} H_2O_2 + O_2 \quad (7b)$$

The self-reaction of HO_2 is dependent on temperature and pressure as well as the presence of water, with recommended rate coefficients of $k_{7a} = (1.6 \pm 0.6) \times 10^{-12}$ and $k_{7b} = (1.3 \pm 0.5) \times 10^{-12}$ cm^3 $molecule^{-1}$ s^{-1} at 298 K and atmospheric pressure.[22–24] When studying the cross-reaction of CH_3O_2 + HO_2 radicals within a chamber, reactions (4), (6), and (7) need to be considered along with potential wall losses of both radicals.

The cross-reaction of CH_3O_2 + HO_2 takes place via two reaction channels:

$$CH_3O_2 + HO_2 \rightarrow CH_3OOH + O_2 \quad (8a)$$

$$CH_3O_2 + HO_2 \rightarrow CH_2O + H_2O + O_2 \quad (8b)$$

Despite the central nature of reaction (8) to atmospheric oxidation, a high uncertainty of 40%–70%

is associated with the kinetics of this reaction, over the temperature range of 260–350 K.[12–15,25–30] However, IUPAC and JPL recommended values agree, at T = 298 K, k_8 = (5.2 ± 1.2) × 10^{-12} and (5.2 ± 2.5) × 10^{-12} cm^3 $molecule^{-1}$ s^{-1}, for IUPAC[12] and JPL,[13] respectively, and the temperature dependent rate coefficients from IUPAC and JPL are described by $k_{8,IUPAC}(T = 205–580\ K) = 3.8 \times 10^{-13} \times \exp((780 \pm 200)/T)$ and $k_{8,JPL}(T = 228–700\ K) = 4.1 \times 10^{-13} \times \exp((750 \pm 150)/T)$ cm^3 $molecule^{-1}$ s^{-1}, respectively.[12,13] Most of the previous studies were based on UV-absorption spectroscopy, using flash photolysis (FP)[25–28] and molecular modulation (MM) methods,[14,15,29] and one study using chemical ionization mass spectrometry (CIMS).[30] The branching of the two reaction channels have recommended values of $\alpha_{8a} = k_{8a}/k_8 = 0.9 \pm 0.1$ and $\alpha_{8b} = k_{8b}/k_8 = 0.1 \pm 0.1$ at 298 K, however, note the uncertainty.[12,31–33] The recommendation by JPL is a product yield of CH_2O of 0, with channel (8a) being the sole reaction channel. Theoretical ab initio investigations of reaction (8) using different levels of theory (density functional theory, Møller-Plesset perturbation [MP] theory, and coupled cluster [CC] theory) found agreement with the temperature dependence,[34–36] but only one study using MP and CC theories found both reaction channels (8a) and (8b).[34] The other theoretical studies found that channel (8a) is the only reaction channel.[13,34–36] Both the IUPAC and JPL recommendations state the need to confirm the product yield of reaction (8b) to determine the branching ratio of the reaction channels.[12,13]

Here we present a determination of the rate coefficient of the reaction of $CH_3O_2 + HO_2$ at a pressure of 1000 mbar of synthetic air and temperatures ranging between 268–344 K in the Highly Instrumented Reactor for Atmospheric Chemistry (HIRAC).[37,38] The Fluorescence Assay by Gas Expansion (FAGE) method was used to detect both radicals selectively and sensitively.[39–41] The method consists of titrating CH_3O_2 or HO_2 radicals with NO to CH_3O or OH radicals, respectively, as shown in reactions (3) and (5), that are then detected by laser induced fluorescence (LIF) with laser excitation at ca. 298 or 308 nm, respectively.[41–43] In fieldwork, FAGE is commonly used for detection of OH and HO_2 radicals[42,44] and has been validated previously for detection of CH_3O_2 in comparison with the direct and absolute method of the near-IR Cavity Ring-Down Spectroscopy (CRDS).[39,40] The rate coefficient of the cross-reaction of CH_3O_2 + HO_2, k_8, is derived using a kinetic model to fit the experimental data with the results compared to the recommended rate coefficient of this reaction by both the IUPAC and JPL kinetic data panels.

2 | EXPERIMENTAL METHODS

2.1 | The Highly Instrumented Reactor for Atmospheric Chemistry (HIRAC)

The Highly Instrumented Reactor for Atmospheric Chemistry (HIRAC) is a 2.25 m^3 stainless steel chamber and is described in detail elsewhere.[37–41] Eight quartz tubes are mounted radially inside the chamber and hold the UV lamps (Phillips, TL-D36W/BLB, λ = 350–400 nm) used for initializing the photochemistry along with four circulation fans to ensure homogeneous mixing of the gas content of the chamber. To perform experiments at varying temperatures from room temperature, a thermofluid (HUBE6479 DW-therm oil) was circulated using a high capacity thermoregulator (Huber Unistat 390 W) in stainless steel tubes on the outside chamber surface. The steel tubes are evenly distributed on the chamber surface and HIRAC is covered in a layer of 20 mm neoprene to ensure a homogeneous temperature across the chamber. The radial and longitudinal variation is <1 K. The temperature uncertainty is ±0.5 K determined as the statistical error of the average temperature measured by five type K thermocouples.

Experiments were performed at 268, 284, 295, 323, and 344 K. All experiments were carried out in 1000 mbar of synthetic air, obtained by mixing high purity O_2 (>99.999%, BOC) and N_2 (>99.998%, BOC) in a ratio of O_2:N_2 = 1:4. CH_4 (99.5%, BOC, CP grade), CH_3OH (≥99.9%, Sigma–Aldrich, HPLC grade), and Cl_2 (≥99.5%, Sigma–Aldrich) were delivered to the chamber in the gas phase using a vacuum line delivery system, resulting in initial concentrations of $[CH_4]_0$ = (2.5–3.0) × 10^{17} molecule cm^{-3}, $[CH_3OH]_0$ = (0.9–5.8) × 10^{14} molecule cm^{-3}, and $[Cl_2]_0$ = (1.3–8.2) × 10^{14} molecule cm^{-3}, yielding initial radical concentrations of $[CH_3O_2]_0$ = (0.8–3.5) × 10^{11} molecule cm^{-3}, and $[HO_2]_0$ = (1.2–6.9) × 10^{10} molecule cm^{-3}, with varying ratios of the initial concentrations of the generated CH_3O_2 and HO_2 radicals of $[CH_3O_2]_0/[HO_2]_0$ = 3–14. After addition of the reagents, photochemistry was initiated by photolysis of molecular chlorine, Cl_2, to Cl atoms that react with CH_4 and O_2 to form CH_3O_2 radicals via reactions (9)–(10) and (2):

$$Cl + h\nu\,(365nm) \rightarrow 2Cl \quad (9)$$

$$CH_4 + Cl \rightarrow CH_3 + HCl \quad (10)$$

$$CH_3 + O_2 \xrightarrow{M} CH_3O_2 \quad (2)$$

Cl atoms will also react with CH_3OH forming CH_2OH that reacts with O_2 to form a peroxy radical

($CH_2(O_2)OH$) that decomposes to yield HO_2 radicals (reactions 11, 12):

$$Cl + CH_3OH \rightarrow CH_2OH + HCl \quad (11)$$

$$CH_2OH + O_2 \rightarrow CH_2O + HO_2 \quad (12)$$

The UV lamps were kept on for typically ~5 min, generating steady state concentrations of the radicals and then turned off allowing the radical concentrations to decay, recording the generated CH_3O_2 or HO_2 kinetic decays. The chamber was kept dry and the concentration of CH_3OH was kept low (compared to other reagents) in all experiments to avoid complications of the reactants reacting with CH_3OH or H_2O. The HIRAC Fourier Transform Infrared (FTIR) spectrometer was used to check for possible impurities in the gases delivered to the chamber, none were detected.

2.2 | The Fluorescence Assay by Gas Expansion (FAGE) instrument

The HIRAC FAGE instrument is described in detail in previous publications.[39–41] It samples the chamber gas mixture through a 1 mm pinhole of a 50 mm internal diameter flowtube at a rate of ~3 SLM, maintaining a flowtube pressure of 3.3 mbar for the 1000 mbar chamber pressure of synthetic air. CH_3O and OH fluorescence detection cells are integrated into the tube at ~600 and ~300 mm from the pinhole, respectively. About 25 mm prior to each detection cell, high purity NO (N2.5 nitric oxide, BOC) was injected at 2.5 sccm into the center of the gas flow using mass flow controllers (Brooks 5850S) to convert CH_3O_2 and HO_2 radicals to CH_3O and OH radicals, respectively. CH_3O radicals were detected by LIF spectroscopy by directing laser light at $\lambda_{CH3O} = 297.79$ nm to excite the $A^2A_1(\nu_3' = 3) \leftarrow X^2E(\nu_3'' = 0)$ transition of CH_3O radicals. The off-resonant red-shifted LIF signal (320–430 nm) was monitored using photon counting. OH radicals were likewise detected by LIF spectroscopy with the laser light at $\lambda_{OH} \sim 308$ nm using the $Q_1(2)$ rotational line of the $A^2\Sigma^+(\nu' = 0) \leftarrow X^2\Pi_i(\nu'' = 0)$ transition of OH radicals. The on-resonant LIF signal (~308 nm) was again monitored using photon counting. For both radicals a 5 kHz pulse repetition frequency of the laser through the detection cell perpendicular to the gas flow was used and the fluorescence of CH_3O or OH radicals was collected by two microchannel plate photomultiplier tubes (MCP-PMT; Photek PMT325/Q/BI/G) equipped with a 50 ns gate unit (Photek GM10-50) for gated photon counting, and the signal was amplified using a preamplifier (Photek PA200-10). For CH_3O radical detection, the laser background was measured at $\lambda_{CH3O} + 2.5$ nm from the online transition, for OH radical detection, the laser background was measured at $\lambda_{OH} - 0.01$ nm. The background was subtracted from the fluorescence signal for both radical detections. Laser light was generated using a using a dye laser (SIRAH Credo-Dye-N) pumped by a pulsed Nd:YAG laser (JDSU Q201HD).

The FAGE method requires calibration to convert the measured fluorescence photon signal to concentrations of CH_3O_2 and HO_2 radicals. This is done by measuring OH or CH_3O from the photolysis of water vapor with or without the presence of CH_4 as described in detail previously.[37–39] Here, we highlight the key steps in the calibration. The OH radicals are generated from photolysis at 184.9 nm of water vapor in synthetic air and sampled with the FAGE instrument:

$$H_2O + h\nu\,(184.9\text{nm}) \rightarrow OH + H \quad (13)$$

$$H + O_2 \rightarrow HO_2 \quad (14)$$

Calibrating CH_3O_2, excess CH_4 (99.5%, BOC, CP grade) was added to the air flow to generate CH_3O_2 from the reaction of OH with CH_4, as shown in reactions (1) and (2), and the resulting air/radical mixture was also sampled with the FAGE instrument. The concentrations of CH_3O_2 and HO_2 were determined by using Equations (1) and (2), respectively:

$$[CH_3O_2] = [OH] = [H_2O] \times \sigma \times \Phi \times F \times t \quad (I)$$

$$[HO_2] = [OH] = [H_2O] \times \sigma \times \Phi \times F \times t \quad (II)$$

where σ is the absorption cross section of water vapor at 184.9 nm, $\sigma = (7.2 \pm 0.2) \times 10^{-20}$ cm^2 molecule^{-1},[45,46] Φ is the photodissociation quantum yield of OH at 184.9 nm (=1), F is the lamp flux at 184.9 nm, which is varied in calibrations to generate different water vapor concentrations, and t is the photolysis time. The product of $F \times t$ was determined by the use of chemical actinometry.[38] In the experiments, calibration factors, C_{CH3O2} and C_{HO2}, were used to determine $[CH_3O_2]$ and $[HO_2]$, as are defined as follows:

$$[CH_3O_2] = S_{CH3O2}/C_{CH3O2} \quad (III)$$

$$[HO_2] = S_{HO2}/C_{HO2} \quad (IV)$$

where S_{CH3O2} and S_{HO2} (counts s^{-1} mW^{-1}) are the recorded signals of CH_3O_2 and HO_2, respectively. Previous studies have shown that the calibration factor for OH does not significantly depend on temperature in the range of 263–344 K,[47,48] so for both radicals, the room temperature

(295 K) calibration factors were used at all temperatures (268–344 K), namely: $C_{CH3O2} = (0.4–1.1) \times 10^{-9}$ and $C_{HO2} = (0.4–2.4) \times 10^{-7}$ counts cm^3 molecule s^{-1} mW^{-1}. The variation in C factor is a result of experiments being carried out over a long period of time; therefore, the calibration factors are matched to the experiment carried out at the same time as the calibration. The calibration of FAGE for both radicals is the main source of uncertainty in the measured rate coefficients as the uncertainty associated with this water vapor method is in the range of 31%–36% for HO_2[38,40] and 34% for CH_3O_2[41] combining systematic and statistical errors at 2σ level. This method of calibration has been used to calibrate FAGE instruments in the field for many years and the reliability of the method has been confirmed by comparison to studies using different instruments[42–44,49–51] as well as in intercomparison of the calibration of both CH_3O_2 and HO_2 radicals to the absolute method of CRDS, finding good agreement between CRDS and FAGE for both radicals.[39,40] The experimental limits of detection (LOD) for the CH_3O_2 and HO_2 radicals are $LOD_{CH3O2} = 1.5 \times 10^9$ molecule cm^{-3} averaged over 120 s and $LOD_{HO2} = 1.5 \times 10^9$ molecule cm^{-3} averaged over 30 s, respectively.

2.3 | Global analysis of CH_3O_2 and HO_2 decays

CH_3O_2 and HO_2 cannot currently be detected at the same time owing to the different wavelengths of the laser being required to detect either CH_3O or OH after conversion by the addition of NO. Hence, the decays of CH_3O_2 and HO_2 radicals were monitored in series by switching between the two detection cells in the FAGE instrument with the laser wavelength tuned to that of either CH_3O or OH. The experiments were performed by first having the lamps in HIRAC switched on to build up steady-state concentration of the radicals, followed by switching the lamps off and monitoring the decay of CH_3O_2 or HO_2 radicals. When fitting the kinetic decays to obtain a rate coefficient for reaction (8) (CH_3O_2 + HO_2), reactions (4), (6), and (7) need to be considered along with possible wall losses. Reaction mixtures of $CH_4/Cl_2/N_2/O_2$ were photolyzed, observing an approximate steady state concentration of CH_3O_2 radicals. The mixture was then left in the dark with no observed loss of reactants or products apart from the loss of CH_3O_2 radicals due to the CH_3O_2 self-reaction as evidenced by fitting an expression to the CH_3O_2 decay based on the self-reaction kinetics. In separate experiments mixtures of $CH_3OH/Cl_2/N_2/O_2$ were likewise photolyzed and left in the dark; however, the loss of HO_2 radicals is not accounted for by the self-reaction of HO_2 radicals alone. An expression fitting the HO_2 decay based on the self-reaction kinetics alone does not fit the data well and a minor wall loss of HO_2 radicals is therefore included in the analysis. Using a kinetic model consisting of the central reactions, where all rate coefficients are fixed except for that of reaction (8), combined with the initial radical concentrations of both radicals, k_8 can be obtained. The reactions included in the model are summarized in Table 1 for the fit of the data at $T = 295$ K using IUPAC and JPL recommendations,[12,13] the rate coefficient and branching ratio (α) of the self-reaction of CH_3O_2, reaction (6), (k_6 and $\alpha_{6b} = k_{6b}/k_6$) from Onel et al.,[11] and the experimentally determined HO_2 heterogeneous loss to the walls from an HO_2 self-reaction experiment performed in HIRAC. Using different initial CH_4 and CH_3OH concentrations, a range of initial concentrations, $[CH_3O_2]_0$ and $[HO_2]_0$, were generated for each radical decay over the course of the experiments. A CH_3O_2 steady-state period and subsequent decay is shown in Figure 1 for an experiment at 295 K. As the CH_3O_2 and HO_2 radicals are not measured simultaneously, an interpolation procedure was used to compute the initial concentration of the other radical for each measured decay. The details about this procedure can be found in the Supplementary Information (SI).

The CH_3O_2 and HO_2 decays are fitted globally for each of the individual temperatures studied here with the kinetic numerical model implemented in the MATLAB software[52–54] following the same method as described by

TABLE 1 Rate coefficients of the reactions included in the kinetic numerical model for the global fitting in MATLAB.

Reaction	k (molecule^{-1} cm^3 s^{-1})	Reference
$CH_3O_2 + CH_3O_2 \rightarrow CH_3OH + CH_2O + O_2$	1.33×10^{-13}	Onel et al.[11]
$CH_3O_2 + CH_3O_2 \rightarrow CH_3O + CH_3O + O_2$	6.85×10^{-14}	Onel et al.[11]
$CH_3O + O_2 \rightarrow CH_2O + HO_2$	1.85×10^{-15}	Burkholder et al.[13]
$CH_3O_2 + HO_2 \rightarrow$ Products	k_8, floated	Initial value from Atkinson et al.[12]
$HO_2 + HO_2 \rightarrow H_2O_2 + O_2$	2.98×10^{-12}	Atkinson et al.[12]
$HO_2 \rightarrow$ Loss	0.0745[a]	Experimental, this study
$CH_3O_2 \rightarrow$ Loss	0[a]	Experimental, this study

Shown here is an example of the model at $T = 295$ K.

[a]Units of s^{-1}. The HO_2 wall loss is determined for each temperature and for different chamber conditions, as the chamber walls may change over time. The wall loss used in the kinetic model is matched to the time of the experiments for each fit.

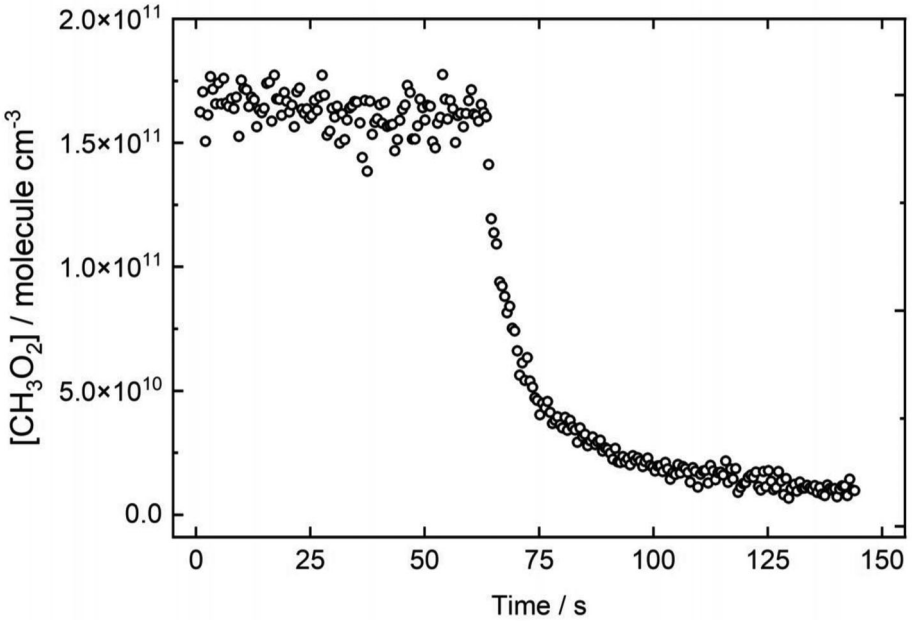

FIGURE 1 Concentration of CH_3O_2 versus time. Between 0 and 65 s the lamps are on, and $[CH_3O_2]$ levels are at an approximate steady state concentration, used as $[CH_3O_2]_0$. At around 65 s, the lamps are turned off, and the CH_3O_2 decays in the dark. The experiment was carried out at 295 K and used 1000 mbar of N_2:O_2 = 4:1 with initial concentrations of $[CH_4]_0 = 2.5 \times 10^{17}$, $[CH_3OH]_0 = 2.7 \times 10^{14}$, and $[Cl_2]_0 = 2.8 \times 10^{14}$ molecule cm^{-3}. Note that the small decrease in $[CH_3O_2]$ during the lamps on period is due to a small gradual decrease of lamp intensity during the initial part of the period, when the lamps are on.

Medeiros et al.[55] Here, all CH_3O_2 and HO_2 decays for all initial concentrations for a given temperature are fitted together, with the rate coefficient of reaction (8) floated, optimizing the fit based on all experimental data. This method takes advantage of using all the available data to better constrain and describe the parameters of the system compared to fitting each decay individually, this process will in most cases improve the standard deviations of the resulting rate coefficients. Each decay is weighted in the global fits to ensure equal representation in the fit regardless of initial radical concentration, this procedure is described in detail in the SI. For each temperature, the global fits have all rate coefficients in Table 1 at fixed values, except k_8 that is floated in the model using the IUPAC recommended value ± two orders of magnitude as the initial guess and boundaries. In the kinetic model, values reported in Onel et al.[11] for the rate coefficient and branching ratio of reaction (6) were used. However, global fits have also been performed with the rate coefficient and branching ratio recommended by IUPAC at all temperatures, exploring the parameters best describing the experimental data.

3 | RESULTS AND DISCUSSION

Figure 2 shows examples of the global fits for decays of CH_3O_2 (panel A) and HO_2 (panel B) radicals after the lamps are turned off. Decays and fits to the decays of both radicals are shown here for a variety of temperatures and initial radical ratios $[CH_3O_2]_0/[HO_2]_0$, encompassing the ranges of radical concentrations and temperatures studied here. All radical decays at each temperature contribute to the global fit of the rate coefficient of reaction (8) and at all individual temperatures, decays of both radicals are included in the fit.

Figure 3 shows the rate coefficient of the reaction of CH_3O_2 with HO_2, k_8, obtained here using a global fit of the data at each temperature (blue and black) versus temperature compared to the recommended values by IUPAC (teal) and JPL (red) at 298 K as well as the recommended temperature dependent rate coefficients (dashed lines) with associated uncertainty ranges represented by the shading for the experimental range of temperatures T = 268–344 K. The temperature dependent recommended values are summarized in Table 2, along with values obtained from the global fit to the data. The global fit using the CH_3O_2 self-reaction rate coefficient determined by Onel et al.[11] (black) gives $k_8 = (4.6 \pm 0.7) \times 10^{-12}$ cm^3 $molecule^{-1}$ s^{-1} at 295 K and the temperature dependent rate coefficient to be $k_{8,\text{Onel-CH3O2-self}}(T) = (5.1 \pm 2.1) \times 10^{-13} \times \exp((637 \pm 121)/T)$ cm^3 $molecule^{-1}$ s^{-1} consistent with the negative temperature dependence for the reaction of CH_3O_2 + HO_2 reported previously.[12,13] The values of k_8 obtained from the global fit of the data (using the rate coefficient and branching ratio of reaction 6 from

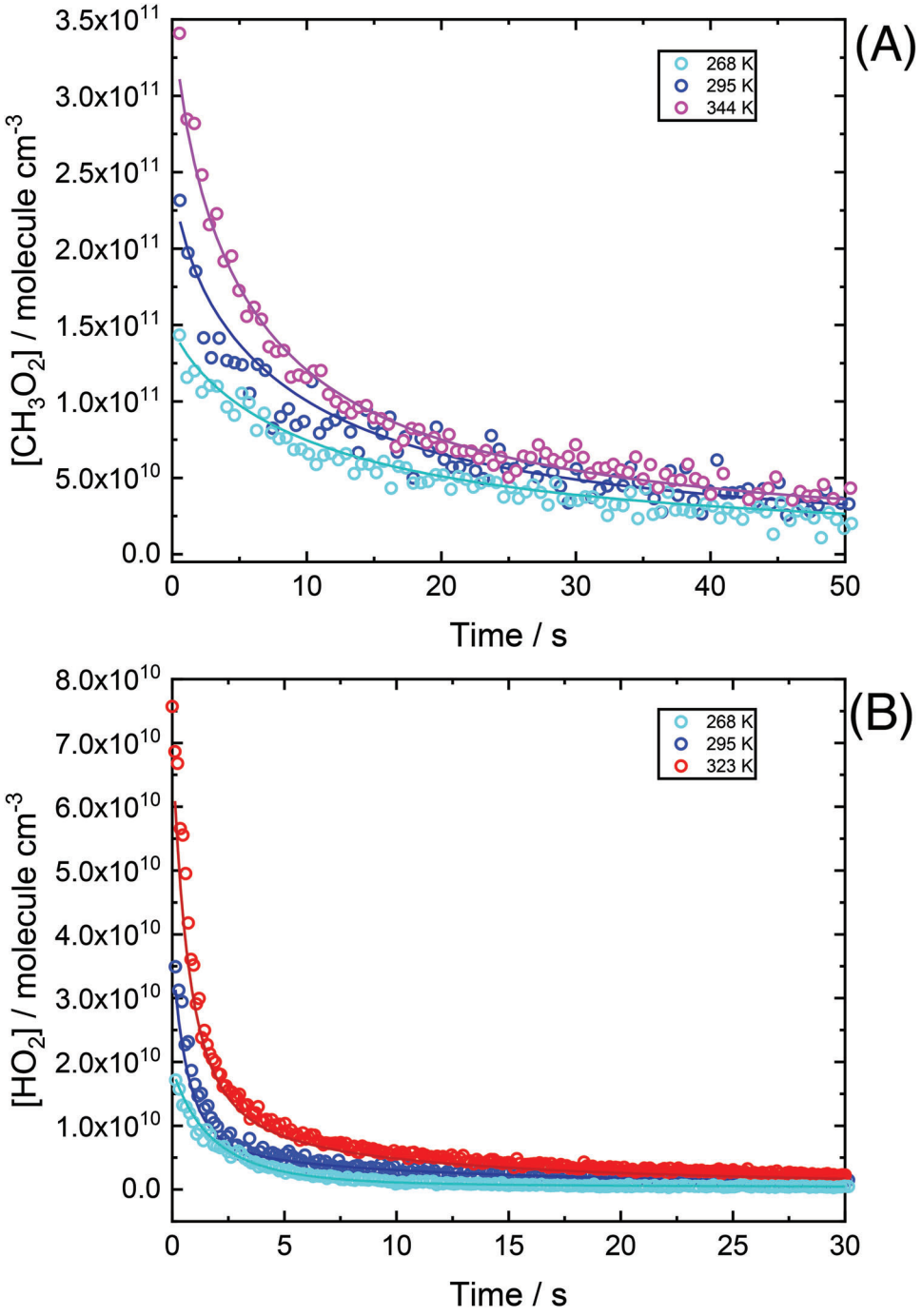

FIGURE 2 Observed experimental radical decays (open circles) of CH_3O_2 (panel A) and HO_2 (panel B) radicals versus time after the lamps were turned off (at $t = 0$ s) for decays highlighting the range of initial radical concentrations across all temperatures studied here. The lines are the fits to the data obtained using the global fitting of the kinetic model as described by the mechanism given in Table 1, see text and the SI for details. All experiments were performed at 1000 mbar of synthetic air: N_2:O_2 = 4:1. Colors indicate the temperature employed in the experiments shown here: 268 K (cyan), 295 K (blue), 323 K (red), and 344 K (magenta). The initial concentrations used were $[CH_4]_0 = (2.5–3.0) \times 10^{17}$, $[CH_3OH]_0 = (2.7–4.9) \times 10^{14}$, and $[Cl_2]_0 = (1.3–8.2) \times 10^{14}$ molecule cm^{-3}.

Onel et al.[11]) from the experiments at 268–344 K are collated in Table 3 along with the literature recommendation values calculated using the temperature dependent Arrhenius equations at the temperatures studied here.[12,13]

Using the IUPAC recommended values[12] for reaction (6) in the global fit (blue), the temperature dependent rate coefficient can be described as $k_{8,\text{IUPAC-CH3O2-self}}(T) = (1.7 \pm 1.2) \times 10^{-12} \times \exp((346 \pm 196)/T)$ cm^3 molecule^{-1} s^{-1}. The fitted rate coefficients

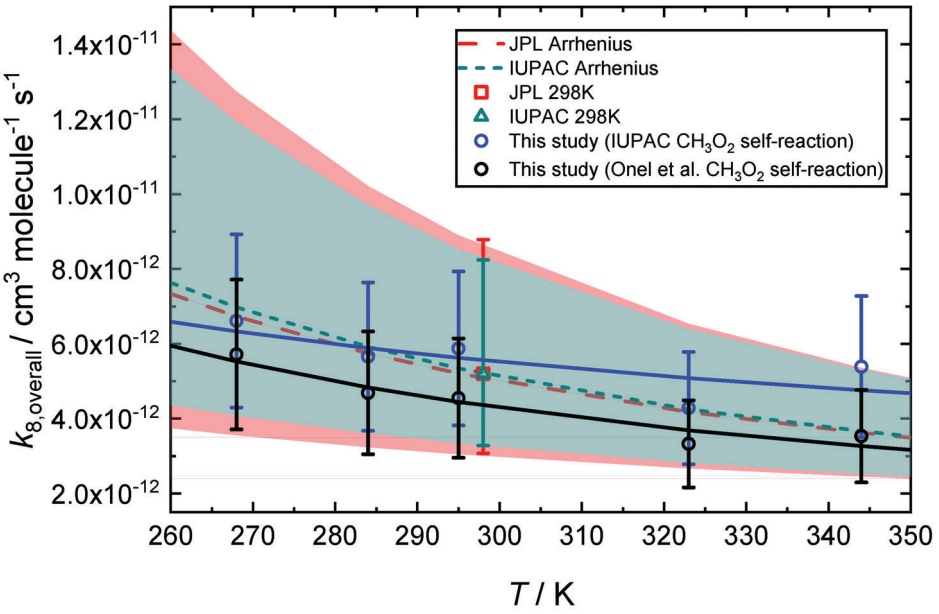

FIGURE 3 Rate coefficient of the $CH_3O_2 + HO_2$ reaction (k_8, molecule^{-1} cm^3 s^{-1}) versus temperature (K). The measured rate coefficients (circles) are shown along with the recommended values by the International Union of Pure and Applied Chemistry (IUPAC, teal triangle) and Jet Propulsion Laboratory (JPL, red square) at 298 K. The measured rate coefficients as described by Arrhenius equations (solid lines) along with the recommended Arrhenius equations (dashed lines) with the uncertainties indicated by the shading for IUPAC (teal) and JPL (red), respectively. The global fit has been performed for each temperature, using the IUPAC recommended CH_3O_2 self-reaction (reaction 6) rate coefficient and branching ratio[12] (blue) and the rate coefficient and branching ratio recently updated by Onel et al.[11] (black). The fit to the data represents the temperature dependence of the rate coefficient, described by $k_8(T) = (5.1 \pm 2.1) \times 10^{-13} \times \exp((637 \pm 121)/T)$ cm^3 molecule^{-1} s^{-1} for the global fitting using the Onel et al. rate coefficient and branching ratio for reaction (6). The measured uncertainty represents a 2σ uncertainty in the global fit as well as experimental uncertainty, see text for details.

TABLE 2 Measured values of the determined temperature dependent rate coefficient of reaction (8), $CH_3O_2 + HO_2$, k_8, at 268–344 K compared to the literature temperature dependent rate coefficients recommended by IUPAC[10] and JPL[11].

Range of T (K)	$k_8(T)$ (cm^3 molecule^{-1} s^{-1})	Reference
205–580	$3.8 \times 10^{-13} \times \exp((780 \pm 200)/T)$	Atkinson et al.[12]
228–700	$4.1 \times 10^{-13} \times \exp((750 \pm 150)/T)$	Burkholder et al.[13]
268–344	$(5.1 \pm 2.1) \times 10^{-13} \times \exp((637 \pm 121)/T)$	This study, CH_3O_2 self-reaction k_6 from Onel et al.[11]
268–344	$(1.7 \pm 1.2) \times 10^{-12} \times \exp((346 \pm 196)/T)$	This study, CH_3O_2 self-reaction k_6 from Atkinson et al.[12]

JPL, Jet Propulsion Laboratory; IUPAC, International Union of Pure and Applied Chemistry.

TABLE 3 Measured values of the determined rate coefficient of reaction (8), $CH_3O_2 + HO_2$, k_8, using the Onel et al.[11] values for reaction (6) at 268–344 K compared to the literature values recommended by IUPAC[12] and JPL.[13]

		Literature k_8 (molecule^{-1} cm^3 s^{-1})	
T (K)	Measured k_8 (molecule^{-1} cm^3 s^{-1})	IUPAC	JPL
268	$(5.7 \pm 0.9) \times 10^{-12}$	$(7.0\ ^{+4.9}_{-2.9}) \times 10^{-12}$	$(6.7\ ^{+6.0}_{-3.2}) \times 10^{-12}$
284	$(4.7 \pm 0.7) \times 10^{-12}$	$(5.9\ ^{+3.8}_{-2.3}) \times 10^{-12}$	$(5.8\ ^{+4.5}_{-2.5}) \times 10^{-12}$
295	$(4.6 \pm 0.7) \times 10^{-12}$	$(5.4\ ^{+3.2}_{-2.0}) \times 10^{-12}$	$(5.2\ ^{+3.7}_{-2.2}) \times 10^{-12}$
323	$(3.3 \pm 0.5) \times 10^{-12}$	$(4.3\ ^{+2.2}_{-1.4}) \times 10^{-12}$	$(4.2\ ^{+2.4}_{-1.5}) \times 10^{-12}$
344	$(3.5 \pm 0.5) \times 10^{-12}$	$(3.7\ ^{+1.7}_{-1.1}) \times 10^{-12}$	$(3.6\ ^{+1.7}_{-1.2}) \times 10^{-12}$

JPL, Jet Propulsion Laboratory; IUPAC, International Union of Pure and Applied Chemistry.

at each temperature are spread both higher and lower than the recommended values for k_8. The values for the A-factor and E_a/R from the Arrhenius equation ($k_{8,\text{IUPAC-CH3O2-self}}(T)$) are further from the recommended values for these two factors ($k_{8,\text{IUPAC}}(T)$[12] and $k_{8,\text{JPL}}(T)$[13]), with no overlap of the ranges of uncertainty, compared to the fit using the Onel et al. CH_3O_2 self-reaction values,[11] even if the computed rate coefficients using the IUPAC values for the CH_3O_2 self-reaction at the specific temperatures have values typically closer to the recommended values for k_8. The uncertainties associated with the recommended temperature dependent rate coefficients presented in Table 3 are asymmetric with the upper uncertainties higher than the lower uncertainties as well as increasing with decreasing temperatures for both recommendations. Figure 3 includes these asymmetric uncertainty ranges of the recommendations by IUPAC and JPL. The two global fits presented in Figure 3 show the same temperature dependent trend. However, the Arrhenius equation obtained using the IUPAC recommended value for the CH_3O_2 self-reaction is associated with a lower quality fit with the $R^2 = 0.51$, whereas the Arrhenius equation obtained, when using the CH_3O_2 self-reaction values from Onel et al.[11] in the global fitting has an $R^2 = 0.90$. Adding to the discussion above, the global fit using the values for k_6 determined by Onel et al.[11] is preferred.

The uncertainties of the experimental values represent a 2σ uncertainty level propagating the experimental uncertainty with the 2σ standard deviation of the global fit. The uncertainty comprises mostly of the experimental uncertainty associated with the calibration of the FAGE instrument of an overall 2σ 31%–36% uncertainty, as reported previously for C_{CH3O2} and C_{HO2} (water vapor method).[38,40,41] The uncertainty of the global fit itself is minor (0.5%–0.9%) compared to this. For all temperatures employed, the uncertainty ranges determined experimentally here are narrower compared to the IUPAC and JPL recommended values. Also, values of k_8 determined here using the global fitting with the Onel et al.[11] CH_3O_2 self-reaction values at each temperature are below the previously reported values. The results reported in this work are between 4–22% and 3–18% lower than the values recommended by IUPAC and JPL, respectively, dependent on temperature, with an average of 16% and 14% lower than IUPAC and JPL values, respectively, for the temperatures studied here. Comparing the rate coefficient for the room temperature experiment at 295 K, the value reported here is 15% and 13% lower than the IUPAC and JPL recommendations, respectively. The IUPAC recommendation of the rate coefficient of reaction (8) is based on the averages of the reported studies at 298 K and the temperature dependence is based on the studies by Lightfoot et al.[28] and Raventós-Duran et al.,[30] whereas the JPL recommendation for both the rate at 298 K and the temperature dependence is based on the evaluated review by Tyndall et al.[9] However, all these studies are in good agreement within the ranges of uncertainty.

Overall, better global fits of the experimental data were obtained for each temperature using the values for k_6 for the CH_3O_2 self-reaction reported by Onel et al.[11] (black), compared to using the IUPAC recommendations (blue), averaged across all temperatures. Using the Onel et al. values improve the global fit by ~15% compared to using the IUPAC values. Onel et al. discuss in detail the discrepancies between the recommended rate coefficient for reaction (6) and their explanation is based on numerical simulations performed by revisiting the methods and findings in the studies on which the IUPAC[12] and JPL[13] recommendations are founded.[14–21] The main conclusions include that the previous studies may be impacted by secondary chemistry, due to high radical concentrations in the experiments, additional wall losses not accounted for, and interferences in absorption spectra by formed products. Some of these factors may play a role for the differences observed here with the recommended values for k_8 as most of the previous studies of reaction (8) are also based on UV spectroscopy and used similar methodology to the studies of reaction (6), namely FP[16–20] and MM.[14,15,21] The exceptions are the study by Raventós-Duran et al.[30] that uses CIMS and reports a value for k_8 in agreement with the IUPAC and JPL recommendations and the study by Jenkin et al.[15] that uses a combination of UV absorption spectroscopy to detect CH_3O_2 radicals and an IR diode laser detection method for HO_2 radicals. All the previous studies of reaction (8) used much higher radical concentrations compared to the present study (as was the case for reaction 6 discussed in Onel et al.[11]) of 1–4 orders of magnitude higher concentrations for both radicals with $[CH_3O_2]_0$ and $[HO_2]_0 \sim 10^{12}$–10^{14} molecule cm^{-3}.[14,15,25–30] These studies relied on using the rate coefficient of reaction (6) in the analysis of experimental data with values either from the older IUPAC and JPL recommendations or studies in agreement with these recommendations. Most studies employ a kinetic model or computer simulation to obtain the rate coefficient for reaction (8). Changing the rate coefficient used for the rate of reaction (6) in the analysis in the previous studies of reaction (8) would decrease the reported rate coefficients of the previous studies of reaction (8), yielding a better agreement with the global fit obtained here using the Onel et al.[11] values for reaction (6). The $CH_3O_2 + HO_2$ reaction rate coefficient should therefore be the lower value obtained here, using the updated CH_3O_2 self-reaction rates determined in Onel et al.[11] associated with the best quality of fit.

4 | CONCLUSIONS

For experiments at 268–344 K at 1000 mbar synthetic air (N_2:O_2 = 4:1) both CH_3O_2 and HO_2 radicals were observed by FAGE in the same reaction mixture in HIRAC. A rate coefficient of the reaction of CH_3O_2 + HO_2, reaction (8) is found to be $k_8(295\ K) = (4.6 \pm 0.7) \times 10^{-12}$ molecule^{-1} cm^3 s^{-1} in agreement with the literature recommendations within the ranges of uncertainty. This study reduces the recommended values slightly by 14%–16%, compared to JPL[13] and IUPAC[12] recommendations, respectively, based on the update to the CH_3O_2 self-reaction rate coefficient as described by Onel et al.[11] The negative temperature dependence reported previously, is confirmed, finding a temperature dependent rate coefficient of $k_8(T) = (5.1 \pm 2.1) \times 10^{-13} \times \exp((637 \pm 121)/T)$ cm^3 molecule^{-1} s^{-1} for the temperature range studied here: T = 268–344 K. The uncertainty ranges for the rate coefficient have been improved significantly by a factor of 1–2, depending on the temperature, compared to the previous recommendations for all temperatures investigated here. In clean atmospheric environments, the dominant loss of CH_3O_2 is through the reaction of CH_3O_2 + HO_2, modeling has estimated that about a third of the CH_3O_2 radicals are removed through reaction with HO_2 in a tropical remote location.[5] An average reduction in the rate coefficient of 14%–16%, as observed in the present study, compared to the currently recommended values[12,13] would result in an increased atmospheric concentration of CH_3O_2 calculated in models, currently = (0.5–6) × 10^8 molecule cm^{-3}.[4–6] Although the concentration of HO_2 radicals is not expected to be significantly impacted by lowering the rate coefficient of the CH_3O_2 + HO_2 reaction as the HO_2 + HO_2 reaction (7) is more important for the loss of HO_2 in clean environments, its lifetime will be longer, and this should be taken in account in models.

ACKNOWLEDGMENTS

The authors would like to thank the Natural Environment Research Council (NERC) for funding (grant reference NE/M011208/1) and the National Centre for Atmospheric Science. A.B. thanks to NERC for a studentship awarded in the framework of the SPHERES doctoral training programme (NE/L002574/1). F.F.Ø. thanks the Carlsberg Foundation for support through the Carlsberg Foundation Internationalisation Fellowship, grant numbers CF16-0493 and CF17-0608. The authors wish to thank Diogo J. Medeiros for helpful discussion about global analysis and assistance in setting up the MATLAB code to perform the global analysis.

DATA AVAILABILITY STATEMENT

The data that support the findings of this study are available from the corresponding author upon reasonable request.

ORCID

Freja F. Østerstrøm https://orcid.org/0000-0003-4125-3365

Paul W. Seakins https://orcid.org/0000-0002-4335-8593

REFERENCES

1. Zador J, Taatjes CA, Fernandes RX. Kinetics of elementary reactions in low-temperature autoignition chemistry. *Prog Energy Combust Sci*. 2011;37(4):371.
2. Kohse-Hoinghaus K. Combustion in the future: the importance of chemistry. *Proc Combust Inst*. 2021;38(1):1.
3. Orlando JJ, Tyndall GS. Laboratory studies of organic peroxy radical chemistry: an overview with emphasis on recent issues of atmospheric significance. *Chem Soc Rev*. 2012;41(19):6294.
4. Whalley LK, Edwards PM, Furneaux KL, et al. Quantifying the magnitude of a missing hydroxyl radical source in a tropical rainforest. *Atmos Chem Phys*. 2011;11(14):7223.
5. Whalley LK, Furneaux KL, Goddard A, et al. The chemistry of OH and HO_2 radicals in the boundary layer over the tropical Atlantic Ocean. *Atmos Chem Phys*. 2010;10(4):1555.
6. Whalley LK, Stone D, Dunmore R, et al. Understanding in situ ozone production in the summertime through radical observations and modelling studies during the Clean air for London project (ClearfLo). *Atmos Chem Phys*. 2018;18(4):2547.
7. World Health Organization. *WHO Global Air Quality Guidelines: Particulate Matter (PM2.5 and PM10), Ozone, Nitrogen Dioxide, Sulfur Dioxide and Carbon Monoxide*. World health Organization; 2021.
8. Whalley LK, Slater EJ, Woodward-Massey R, et al. Evaluating the sensitivity of radical chemistry and ozone formation to ambient VOCs and NO_x in Beijing. *Atmos Chem Phys*. 2021;21(3):2125-2147. doi:10.5194/acp-21-2125-2021
9. Tyndall GS, Cox RA, Granier C, et al. Atmospheric chemistry of small organic peroxy radicals. *J Geophys Res Atmos*. 2001;106(D11):12157.
10. Tyndall GS, Wallington TJ, Ball JC. FTIR product study of the reactions CH_3O_2+CH_3O_2 and CH_3O_2+O_3. *J Phys Chem A*. 1998;102(15):2547.
11. Onel L, Brennan A, Østerstrøm FF, et al. Kinetics and product branching ratio study of the CH_3O_2 self-reaction in the highly instrumented reactor for atmospheric chemistry. *J Phys Chem A*. 2022;126(42):7639-7649. doi:10.1021/acs.jpca.2c04968
12. Atkinson R, Baulch DL, Cox RA, et al. Evaluated kinetic and photochemical data for atmospheric chemistry: volume II – gas phase reactions of organic species. *Atmos Chem Phys*. 2006;6(11):3625-4055. doi:10.5194/acp-6-3625-2006
13. Burkholder JB, Sander SP, Abbatt J, et al. *Chemical Kinetics and Photochemical Data for Use in Atmospheric Studies, Evaluation No. 19*. Jet Propulsion Laboratory; 2019. http://jpldataeval.jpl.nasa.gov

14. Cox RA, Tyndall GS. Rate constants for the reactions of CH_3O_2 with HO_2, NO and NO_2 using molecular modulation spectrometry. *J Chem Soc, Faraday Trans 2*. 1980;76:153.
15. Jenkin ME, Cox RA, Hayman GD, Whyte LJ. Kinetic study of the reactions CH_3O_2 + CH_3O_2 and CH_3O_2 + HO_2 using molecular modulation spectroscopy. *J Chem Soc, Faraday Trans 2*. 1988;84:913.
16. Kurylo MJ, Wallington TJ. The temperature dependence of the rate constant for the gas phase disproportionation reaction of CH_3O_2 radicals. *Chem Phys Lett*. 1987;138(6):543.
17. Lightfoot PD, Lesclaux R, Veyret B. Flash photolysis study of the CH_3O_2 + CH_3O_2 reaction: rate constants and branching ratios from 248 to 573 K. *J Phys Chem*. 1990;94(2):700.
18. McAdam K, Veyret B, Lesclaux R. UV absorption spectra of $HO_2$and CH_3O_2 radicals and the kinetics of their mutual reactions ant 298 K. *Chem Phys Lett*. 1987;133(1):39.
19. Sander SP, Watson RT. Kinetic studies of the reactions of CH_3O_2 with NO, NO_2 and CH_3O_2 at 298 K. *J Phys Chem*. 1980;84(13):1664.
20. Sander SP, Watson RT. Temperature dependence of the self-reaction of CH_3O_2 radicals. *J Phys Chem*. 1981;85(20):2960.
21. Simon FG, Schneider W, Moortgat GK. UV absorption spectrum of the methylperoxy radical and the kinetics of its disproportionation reaction at 300 K. *Int J Chem Kinet*. 1990;22(8):791.
22. Atkinson R, Baulch DL, Cox RA, et al. Evaluated kinetic and photochemical data for atmospheric chemistry: volume I – gas phase reactions of O_x, HO_x, NO_x and SO_x species. *Atmos Chem Phys*. 2004;4(6):1461-1738. doi:10.5194/acp-4-1461-2004
23. Kircher CC, Sander SP. Kinetics and mechanism of HO_2 and DO_2 disproportionations. *J Phys Chem*. 1984;88:2082-2091.
24. Wallington TJ, Dagaut P, Kurylo MJ. UV absorption cross sections and reaction kinetics and mechanisms for peroxy radicals in the gas phase. *Chem Rev*. 1992;92(4):667-710. doi:10.1021/cr00012a008
25. Boyd AA, Flaud P-M, Daugey N, Lesclaux R. Rate constants for RO_2 + HO_2 reactions measured under a large excess of HO_2. *J Phys Chem A*. 2003;107(6):818-821. doi:10.1021/jp026581r
26. Dagaut P, Wallington TJ, Kurylo MJ. The temperature dependence of the rate constant for the hydroperoxy + methylperoxy gas-phase reaction. *J Phys Chem*. 1988;92(13):3833-3836. doi:10.1021/j100324a030
27. Lightfoot PD, Roussel P, Caralp F, Lesclaux R. Flash photolysis study of the CH_3O_2+ CH_3O_2 and CH_3O_2+ HO_2 reactions between 600 and 719 K: unimolecular decomposition of methylhydroperoxide. *J Chem Soc, Faraday Trans*. 1991;87(19):3213-3220. doi:10.1039/FT9918703213
28. Lightfoot PD, Veyret B, Lesclaux R. Flash photolysis study of the CH_3O_2 + HO_2 reaction between 248 and 573 K. *J Phys Chem*. 1990;94:708-714.
29. Moortgat GK, Cox RA, Schuster G, Burrows JP, Tyndall GS. Peroxy radical reactions in the photo-oxidation of CH_3CHO. *J Chem Soc, Faraday Trans 2*. 1989;85(7):809-829. doi:10.1039/F29898500809
30. Raventós-Duran MT, McGillen M, Percival CJ, Hamer PD, Shallcross DE. Kinetics of the CH_3O_2 + HO_2 reaction: a temperature and pressure dependence study using chemical ionization mass spectrometry. *Int J Chem Kinet*. 2007;39(10):571-579. doi:10.1002/kin.20269
31. Elrod MJ, Ranschaert DL, Schneider NJ. Direct kinetics study of the temperature dependence of the CH_2O branching channel for the CH_3O_2 + HO_2 reaction. *Int J Chem Kinet*. 2001;33:363-376.
32. Wallington TJ. Fourier-transform infrared product study of the reaction of CH_3O_2+ HO_2 over the pressure range 15–700 torr at 295 K. *J Chem Soc Faraday Trans*. 1991;87(15):2379-2382. doi:10.1039/FT9918702379
33. Wallington TJ, Japar SM. Reaction of CH_3O_2+HO_2 in air at 295 K: a product study. *Chem Phys Lett*. 1990;167(6):513-518. doi:10.1016/0009-2614(90)85461-K
34. Drougas E. Quantum mechanical studies of the CH_3O_2 + HO_2 reaction. *Comput Theor Chem*. 2016;1093:98-103. doi:10.1016/j.comptc.2016.08.018
35. Hou H, Wang B. A systematic computational study on the reactions of HO_2 with RO_2: The HO_2 + CH_3O_2 (CD_3O_2) and HO_2 + CH_2FO_2 reactions. *J Phys Chem A*. 2005;109(3):451-460. doi:10.1021/jp046329e
36. Zhou XM, Zhou ZY, Wu QY, Jalbout AF, Zhang N. Reaction of CH_3O_2 and HO_2: ab initio characterization of dimer structure and vibrational mode analysis for reaction mechanisms. *Int J Quantum Chem*. 2006;106(2):514-525. doi:10.1002/qua.20766
37. Glowacki DR, Goddard A, Hemavibool K, et al. Design of and initial results from a Highly Instrumented Reactor for Atmospheric Chemistry (HIRAC). *Atmos Chem Phys*. 2007;7(20):5371.
38. Winiberg FAF, Smith SC, Bejan I, et al. Pressure-dependent calibration of the OH and HO_2 channels of a FAGE HO_x instrument using the Highly Instrumented Reactor for Atmospheric Chemistry (HIRAC). *Atmos Meas Tech*. 2015;8(2):523.
39. Onel L, Brennan A, Gianella M, et al. An intercomparison of CH_3O_2 measurements by fluorescence assay by gas expansion and cavity ring-down spectroscopy within HIRAC (Highly Instrumented Reactor for Atmospheric Chemistry). *Atmos Meas Tech*. 2020;13(5):2441.
40. Onel L, Brennan A, Gianella M, et al. An intercomparison of HO_2 measurements by fluorescence assay by gas expansion and cavity ring-down spectroscopy within HIRAC (Highly Instrumented Reactor for Atmospheric Chemistry). *Atmos Meas Tech*. 2017;10(12):4877.
41. Onel L, Brennan A, Seakins PW, Whalley L, Heard DE. A new method for atmospheric detection of the CH_3O_2 radical. *Atmos Meas Tech*. 2017;10(10):3985.
42. Heard DE, Pilling MJ. Measurement of OH and HO_2 in the troposphere. *Chem Rev*. 2003;103(12):5163-5198.
43. Wang GY, Iradukunda Y, Shi GF, Sanga P, Niu XL, Wu ZJ. Hydroxyl, hydroperoxyl free radicals determination methods in atmosphere and troposphere. *J Environ Sci*. 2021;99:324.
44. Stone D, Whalley LK, Heard DE. Tropospheric OH and HO_2 radicals: field measurements and model comparisons. *Chem Soc Rev*. 2012;41(19):6348.
45. Cantrell CA, Zimmer A, Tyndall GS. Absorption cross sections for water vapor from 183 to 193 nm. *Geophys Res Lett*. 1997;24(21):2195-2198.
46. Creasey DJ, Heard DE, Lee JD. Absorption cross-section measurements of water vapour and oxygen at 185 nm. Implications for the calibration of field instruments to measure OH, HO_2 and RO_2 radicals. *Geophys Res Lett*. 2000;27(11):1651.
47. Regelin E, Harder H, Martinez M, et al. HO_x measurements in the summertime upper troposphere over Europe: a comparison

of observations to a box model and a 3-D model. *Atmos Chem Phys*. 2013;13(21):10703-10720. doi:10.5194/acp-13-10703-2013

48. Winiberg FAF. *Characterisation of FAGE Apparatus for HO_x Detection and Application in an Environmental Chamber*. PhD thesis. University of Leeds; 2014.
49. Dusanter S, Vimal D, Stevens PS. Technical note: measuring tropospheric OH and HO_2 by laser-induced fluorescence at low pressure. A comparison of calibration techniques. *Atmos Chem Phys*. 2008;8(2):321.
50. Fuchs H, Dorn HP, Bachner M, et al. Comparison of OH concentration measurements by DOAS and LIF during SAPHIR chamber experiments at high OH reactivity and low NO concentration. *Atmos Meas Tech*. 2012;5(7):1611.
51. Schlosser E, Brauers T, Dorn HP, et al. Technical note: formal blind intercomparison of OH measurements: results from the international campaign HOxComp. *Atmos Chem Phys*. 2009;9(20):7923.
52. The MathWorks, Inc. (2022). *MATLAB version: 9.13.0 with Optimization Toolbox version: 9.4 (R2022b)*. Accessed: 10 October, 2022. Available: https://www.mathworks.com
53. Moré JJ, Sorensen DC. Computing a trust region step. *SIAM J Sci Stat Comput*. 1983;4(3):553-572. doi:10.1137/0904038
54. Shampine LF, Reichelt MW. The MATLAB ODE suite. *SIAM J Sci Comput*. 1997;18(1):1-22. doi:10.1137/s1064827594276424
55. Medeiros DJ, Blitz MA, Seakins PW, Whalley LK. Direct measurements of isoprene autoxidation: pinpointing atmospheric oxidation in tropical forests. *JACS Au*. 2022;2(4):809-818. doi:10.1021/jacsau.1c00525

SUPPORTING INFORMATION

Additional supporting information can be found online in the Supporting Information section at the end of this article.

How to cite this article: Østerstrøm FF, Onel L, Brennan A, et al. Kinetics of the cross-reaction of CH_3O_2 + HO_2 radicals measured in the Highly Instrumented Reactor for Atmospheric Chemistry. *Int J Chem Kinet*. 2023;55:489–500. https://doi.org/10.1002/kin.21651